Copy No. _____

Defence Research and Development Canada
Recherche et développement pour la défense Canada

DEFENCE R&D DÉFENSE

Analytical Solutions for Predicting Underwater Explosion Gas Bubble Behaviour

Mark Riley

Defence R&D Canada – Atlantic

Technical Memorandum
DRDC Atlantic TM 2010-237
November 2010

Canada

This page intentionally left blank.

Analytical Solutions for Predicting Underwater Explosion Gas Bubble Behaviour

Mark Riley

Defence R&D Canada – Atlantic

Technical Memorandum
DRDC Atlantic TM 2010-237
November 2010

Principal Author

Original signed by Mark Riley

Mark Riley

Defence Scientist WP

Approved by

Original signed by Neil Pegg

Neil Pegg

Section Head WP

Approved for release by

Original signed by Ron Kuwahara for

Calvin Hyatt

DRP Chair

Abstract

This study describes different analytical models that have previously been developed for predicting the radial growth and collapse of underwater explosion (UNDEX) gas bubbles in a free-field environment. The report describes the implementation of nine analytical gas bubble models, in the form of nonlinear differential equations, and a fourth-order Runge-Kutta solution method. Gas bubble radius time histories calculated with these models are compared to empirical models derived from published experimental data. The analytical models allow for different assumptions such as fluid compressibility, bubble migration coupled to dilatation, and an empirical correction for energy loss. It was found that none of the analytical models fully account for the reduction in the gas bubble radius throughout the growth and collapse cycles. Including compressibility in the fluid and the gas bubble provides the best predictions when compared to experimental fits. The incompressible fluid model requires an empirical energy loss function, as there is no energy loss inherent within the model. Models considering just the compressibility of the surrounding fluid do not account for the full energy loss seen in the experimental fits, and produced similar results. Inclusion of migration effects had no influence on the bubble radius or period because of the large detonation depth.

Résumé

La présente étude décrit différents modèles analytiques élaborés antérieurement pour prévoir la croissance et l'implosion radiales en champ libre des bulles gazeuses créées par une explosion sous-marine (UNDEX). Le rapport décrit la mise en œuvre de neuf modèles analytiques de bulles gazeuses utilisant des équations différentielles non linéaires et une méthode de solution de Runge-Kutta du quatrième ordre. On compare l'évolution temporelle du rayon des bulles gazeuses calculée avec ces divers modèles avec celle obtenue avec des modèles empiriques dérivés de données expérimentales publiées. Les modèles analytiques permettent différentes hypothèses concernant, entre autres, la compressibilité du fluide, la migration des bulles reliée à la dilatation, et la correction empirique de la perte d'énergie. On constate qu'aucun des modèles analytiques ne peut expliquer complètement la réduction du rayon des bulles gazeuses sur toute l'étendue des cycles de croissance et d'implosion. L'inclusion des compressibilités du fluide et des bulles gazeuses donne les meilleures prévisions comparativement aux ajustements avec les données expérimentales. Le modèle à fluide incompressible exige d'utiliser une fonction empirique de perte d'énergie étant donné qu'il ne tient pas compte lui-même de la perte d'énergie. Les modèles qui ne tiennent compte que de la compressibilité du fluide environnant ne peuvent expliquer complètement la perte d'énergie observée dans les ajustements aux données expérimentales et donnent des résultats similaires. L'inclusion des effets dus à la migration n'a aucun effet sur le rayon ou la durée des bulles à cause de la grande profondeur à laquelle les explosions ont lieu.

This page intentionally left blank.

Executive summary

Analytical Solutions for Predicting Underwater Explosion Gas Bubble Behaviour

Mark Riley; DRDC Atlantic TM 2010-237; Defence R&D Canada – Atlantic; November 2010.

Introduction: Ship vulnerability to underwater explosion loading is being investigated as part of the Maritime Force Protection (MFP) TDP. The ultimate goal of this project is to deliver a validated capability to predict these types of loading which can then be applied to full scale ships. This study developed a computer code to implement analytical models that will provide a quick and easy way to determine the radial and migration behaviour of an underwater explosion gas bubble. The analytical results are compared to experimental fits.

Results: This report compares various analytical models for predicting the growth and collapse of an underwater explosion gas bubble. The different models use various underlying assumptions such as compressibility of the surrounding fluid and gas bubble, energy losses, and the coupling of radial and migration motion. This study shows that the reduction in gas bubble radius through the growth and collapse cycles is underestimated by all of the analytical models when compared to experiments. Of the models trialed, the best results were obtained when compressibility of the gas and surrounding fluid was included.

Significance: The analytical models trialed in this study are simple alternatives to two dimensional and three-dimensional numerical simulations involving run times up to 14 days on 30-40 processors. Using analytical models, the run time is in the order of seconds for the same simulation time. This study is an initial step in the development of a code that will predict the loading from an underwater explosion gas bubble in close proximity to a target. The results of this study show that there are various underlying assumptions that can be made which significantly affect the gas bubble response.

Future plans: The models implemented in this study could be extended to predict far-field bubble loads on ships and subs for analysis such as whipping. Further development of the code is planned to include the influence of a close proximity target on the behaviour of the gas bubble.

Sommaire

Analytical Solutions for Predicting Underwater Explosion Gas Bubble Behaviour

Mark Riley; DRDC Atlantic TM 2010-237; R & D pour la défense Canada – Atlantique; Novembre 2010.

Introduction : La vulnérabilité des navires à la charge exercée par les explosions sous-marines est actuellement étudiée dans le cadre du Programme de démonstration de technologies (PDT) de protection de la force navale (PFN). Le but ultime du projet est de mettre au point un outil validé permettant de calculer les charges de ce type, puis de l'appliquer à des navires de grandeur nature. La présente étude a élaboré un code machine pour mettre en œuvre des modèles analytiques qui permettront de déterminer rapidement et facilement les comportements radial et migratoire d'une bulle gazeuse créée par une explosion sous-marine. On compare les résultats analytiques avec les ajustements aux données expérimentales.

Résultats : Le présent rapport compare divers modèles analytiques servant à prévoir la croissance et l'implosion d'une bulle gazeuse créée par une explosion sous-marine. Ces modèles font diverses hypothèses concernant, entre autres, les compressibilités du fluide environnant et de la bulle gazeuse, la perte d'énergie, et le couplage des mouvements radial et migratoire. L'étude montre que, comparativement aux résultats d'expérience, la réduction du rayon de la bulle gazeuse dans les cycles de croissance et d'implosion est sous-estimée par tous les modèles analytiques. Parmi les modèles mis à l'essai, on a obtenu les meilleurs résultats quand on a tenu compte des compressibilités du gaz et du fluide environnant.

Importance : Les modèles analytiques mis à l'essai dans la présente étude sont des modèles simples visant à remplacer des simulations numériques bi- et tridimensionnelles d'une durée d'exécution pouvant atteindre 14 jours sur 30 à 40 processeurs. Avec ces modèles analytiques, la durée d'exécution est de l'ordre de quelques secondes. L'étude est un premier pas dans l'élaboration d'un code qui prédira la charge exercée par une bulle de gaz créée par une explosion sous-marine au voisinage immédiat d'une cible. Les résultats de l'étude montrent que l'on peut s'appuyer sur diverses hypothèses et que celles-ci ont un effet important sur le comportement de la bulle gazeuse.

Perspectives : Les modèles élaborés dans la présente étude pourraient être appliqués à la prévision des charges des bulles en champ lointain sur les navires et les sous-marins en vue d'analyser des effets comme le fouettement. On prévoit améliorer le code pour y inclure l'effet d'une cible très proche sur le comportement de la bulle gazeuse.

Table of contents

List of figures

List of tables

1 Introduction

Naval vessels can be subjected to severe blast loading from both air and underwater explosions. For underwater explosions in close proximity to a structure, the loading mechanism is entirely different than for air blast. With underwater explosions, a shock is formed that propagates through the water and loads the structure with a significant pressure pulse. An underwater explosion will also generate a pulsating gas bubble whose size depends on the chemical composition of the explosive, the mass of the charge, and the depth of the charge in the water. When the charge is detonated within 2-3 times the maximum free-field bubble radius, R, of the structure, the bubble collapse and the water jet that is created by the collapse are very likely to be directed at the structure. At even closer ranges the bubble collapses directly onto the structure, resulting in loading that can be more severe than the shock loading. The bubble can then reform and pulsate against the structure, resulting in more loading cycles. During the bubble collapse the boundary of the bubble farthest from the structure typically collapses inward, allowing a water jet directed toward the structure to form and causing the bubble to change from a spherical to toroidal shape as shown in Figure 1.

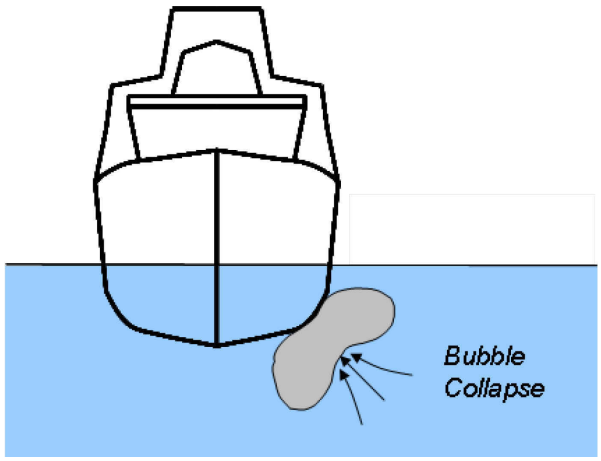

Figure 1: Bubble collapse and water jet formation against a structure

As part of the Maritime Force Protection (MFP) TDP, ship vulnerability to underwater explosion loading is being investigated. The ultimate goal of this project is to deliver a validated capability to predict these types of loading which can then be applied to full scale ships. Although numerical analysis tools are available for modelling the loading and structural response for close-proximity UNDEX, these methods are laborious and very time consuming and still exhibit quantitative gaps when compared to experimental results. This study is an initial step in developing a simplified approach to determining the loading on a structure due to close proximity UNDEX gas bubble collapse.

This report examines various analytical models that are available for predicting the gas bubble growth and collapse. The similitude equations for explosive materials have been shown to provide good results for various shock parameters, such as the peak pressure, decay time, and energy as well as the gas bubble period and maximum free-field gas bubble radius. Major limitations of the similitude equations and current analytical approaches are they do not include effects of loading from the gas bubble collapse, they do not account for the close proximity of a structure and they require an extensive set of constants which depend on the charge material, which can be very difficult to obtain. Another issue with the similitude equations and incompressible fluid analytical models is the lack of energy loss predictions. Various analytical models have been developed in the past to predict the time history behaviour of a free field gas bubble. This report compares the bubble radius time history of a series of analytical models to experimental fit results reported by Swift and Decius [1].

2 Empirical Models

2.1 Similitude Equations

The similitude equation for the first maximum bubble radius [2] is as shown in Eq. (1).

$$R_{\max} = K_6\left(\frac{W}{D+10}\right)^{1/3} \tag{1}$$

where R_{max} is the maximum bubble radius in meters, D is the charge depth in meters, W is the charge weight in kilograms, and K_6 is a constant depending on the charge material. The similitude expression for determining the first bubble period [2], T_b, in seconds is estimated by Eq. (2).

$$T_b = K_5\frac{W^{1/3}}{(D+10)^{5/6}} \tag{2}$$

where K_5 is a constant which depends on the charge material. The rise in the gas bubble over its first bubble period, Δd, is given by Eq. (3), as show by van Aanhold [2]. It should be noted that this is equation is specific to TNT.

$$\Delta d = 12.4\frac{W}{(D+10)} \tag{3}$$

The volume of the gas bubble can be reasonably approximated by a half sine function as shown by Eq. (4), where V_o is the initial charge volume and V_{max} is the maximum bubble volume calculated using the maximum bubble radius assuming a spherical bubble, as shown in Eq. (4).

$$\begin{aligned} V(t) &= V_o + (V_{\max} - V_o)\sin\left(\frac{\pi t}{T_b}\right) \\ V_{\max} &= \frac{4}{3}\pi R_{\max}^3 \end{aligned} \tag{4}$$

From the volume time relation of the bubble the radius time history can be determined by Eq. (5) assuming a spherical gas bubble.

$$R(t) = \left(\frac{3}{4\pi} V(t) \right)^{1/3} \tag{5}$$

The vertical position of the gas bubble center, which describes its vertical migration, can be approximated by Eq. (6).

$$z(t) = -d + \Delta d \cdot \left(1 - \cos\left(\frac{\pi t}{2T_b} \right)^{0.40} \right) \tag{6}$$

2.2 Similitude Model With Energy Loss

This approach used the first cycle period constants with an energy loss function to determine the radial and migration time histories. The energy loss function, given by Eq. (7), was provided by van Aanhold [2], which was based on reduction values used by Geers and Hunter [7].

$$\lambda = 0.2575 + (1 - 0.2575)\exp(-0.8148m) \tag{7}$$

Here λ has an initial value of 1 (m=0), and m is the cycle number starting at 0 for detonation and with m=1 for the first gas bubble minimum. The energy loss function is implemented by reducing the charge mass at each gas bubble minimum, such that the new charge weight is λW. This new charge weight is input into Eqs. (1) through (3) to determine the maximum gas bubble radius, the bubble period, and the migration during the next cycle. This energy loss function results in a decrease in the maximum gas bubble radius and periods by an order of ($\lambda^{1/3}$).

2.3 Experimental Fit Model

The average similitude constants for the charge material used in this study are shown in Table 1.

Table 1: Similitude constants for TNT in MKS units

Constant	TNT		
	1st Cycle	2nd Cycle	3rd Cycle
K_5	2.11	1.57	1.33
K_6	3.36	2.27	1.76

The three sets of constants for TNT are based on an experimental study by Swift and Decius [1], who experimentally measured the radius and period of the gas bubble. The similitude constants were determined as the values producing the best fit to the experimental data. For some experiments the fits were produced for the first three bubble

periods, but for most experiments there were only measurements for the first one or two bubble periods. The experimental set-up and resulting similitude constants for all experiments for TNT are shown in Annex A.

3 Analytical Models

Experimentally it is extremely difficult to monitor the position and radius of the gas bubble created by underwater explosions. Therefore, in order to help validate numerical approaches for solving the gas bubble behaviour, analytical expressions have been derived for predicting the time history of the gas bubble radius and vertical position. Although several approaches are available there are limitations in the predictive models. Like the similitude equations, the analytical models do not predict the influence of a close proximity target. The various equations of motion (EOM) compared in this report include the Rayleigh-Plesset equation which was original developed by Lamb [3], Herring EOM [4], Kirkwood and Bethe (KB) EOM [5], Keller and Kolodner (KK) EOM [6], three EOM developed by Geers and Hunter [7,8,9], and an EOM developed at TNO [2].

3.1 Lamb EOM

The Lamb EOM [3], shown in Eq. (8), was one of the original analytical solutions for predicting the gas bubble radius. This approach assumes the bubble is stationary about its center, such that the gas bubble moves in the radial direction only and has no vertical migration. It assumes the fluid is incompressible and a free-field condition.

$$R\ddot{R} + \frac{3}{2}\dot{R}^2 = \rho_w^{-1}\left(p_{gas} - p_{air} + \rho_w g z\right) \tag{8}$$

Where $R, \dot{R}$ and, $\ddot{R}$ are the instantaneous bubble radius, radial velocity, and radial acceleration respectively, ρ_w is the water density, p_{gas} is the pressure in the gas bubble, p_{air} is the atmospheric pressure, g is gravity, and z is the depth of the charge.

Due to the incompressible fluid formulation of the Lamb EOM there is no energy loss built into the model, therefore an external energy loss function must be applied. The energy loss function is the same factor as that used for the similitude equations, with the loss function λ being applied to the internal gas pressure of the bubble, as shown by Eq. (7) in Section 2.2.

3.2 Herring EOM

The Herring EOM [4], Eq. (9), accounts for wave effects (i.e. compressibility) in the water but not in the gas bubble. The compressibility is accounted for through the addition and inclusion of a finite fluid sound speed, c. By setting the sound speed to infinity, the Herring EOM reduces to the Lamb EOM for an incompressible fluid.

$$R\ddot{R}\left(1-2\frac{\dot{R}}{c}\right)+\frac{3}{2}\dot{R}^2\left(1-\frac{4\dot{R}}{3c}\right)=\rho_w^{-1}\left(p_{gas}-p_{air}+\rho_w gz+\frac{R}{c}\dot{P}_g\right) \tag{9}$$

$\dot{P}_g$ is the first time derivative of the pressure in the gas. With the inclusion of compressibility, energy losses can occur. The most significant energy loss term is the term containing $\dot{P}_g$; the term $\left(1-\frac{4\dot{R}}{3c}\right)$ gives negligible energy loss, but creates an asymmetry in the radius time history, whereby the contraction of the bubble is slower than its growth.

3.3 Kirkwood and Bethe (KB) EOM

Similar to the Herring EOM, the KB EOM [5], Eq. (10), accounts for wave effects in the liquid and can be implemented for either an incompressible or compressible fluid. As this equation shows there is very little difference between this equation and that produced by Herring.

$$R\ddot{R}\left(1-\frac{\dot{R}}{c}\right)+\frac{3}{2}\dot{R}^2\left(1-\frac{\dot{R}}{3c}\right)=\rho_w^{-1}\left(p_{gas}-p_{air}+\rho_w gz+\frac{R}{c}\dot{P}_g\right)\left(1+\frac{\dot{R}}{c}\right) \tag{10}$$

The $\left(1+\frac{\dot{R}}{c}\right)$ term on the right hand side makes a slight difference due to its influence on the damping term containing $\dot{P}_g$. This results from keeping the enthalpy at the bubble surface throughout the derivation, and not using an approximation to the enthalpy as implemented in the Herring and KK EOM. The other terms containing $\left(\frac{\dot{R}}{c}\right)$ produce negligible effects.

3.4 Keller and Kolodner (KK) EOM

The KK EOM [6], Eq. (11), looks similar to the KB model but is very similar in behaviour to that produced by Herring, as the major damping term is the same. The KK EOM accounts for the fluid compressibility by defining a finite value for the speed of sound in the water.

$$R\ddot{R}\left(1-\frac{\dot{R}}{c}\right)+\frac{3}{2}\dot{R}^2\left(1-\frac{\dot{R}}{3c}\right)=\rho_w^{-1}\left(\left(P_g-p_{air}+\rho_w gz\right)\left(1+\frac{\dot{R}}{c}\right)+\frac{R}{c}\dot{P}_g\right) \tag{11}$$

Both the Herring and KK EOM can be grouped into a single one-parameter equation, shown in Eq. (12), which was referred to as the Keller-Herring Equation by Prosperetti and Lezzi [10], where λ is an arbitrary parameter with a value between zero and one.

$$R\ddot{R}\left(1-(\lambda+1)\frac{\dot{R}}{c}\right)+\frac{3}{2}\dot{R}^2\left(1-\frac{1}{3}(3\lambda+1)\frac{\dot{R}}{c}\right)=\rho_w^{-1}\left(\left(P_g-p_{air}+\rho_w gz\right)\left(1+(1-\lambda)\frac{\dot{R}}{c}\right)+\frac{R}{c}\dot{P}_g\right) \tag{12}$$

Setting λ to zero gives the KK EOM; setting λ to 1 gives the Herring EOM.

3.5 Geers and Hunter EOM Models

Over the past decade and a half Geers and Hunters have developed several models to predict the gas bubble behaviour for underwater explosions. For the purposes of this study three EOM variations were used. Two approaches, the DA and coupled DA account for compressibility in the fluid, where the third model, DAA EOM, accounts for wave effects in both the fluid and gas bubble.

3.5.1 GH-DA EOM

For the GH-DA EOM [7], only the dilatational motion of the gas bubble is considered, as given by Eq. (13).

$$R\ddot{R}+\frac{3}{2}\dot{R}^2=\rho_w^{-1}\left(\left(1+\frac{\dot{R}}{c}\frac{d}{dt}\right)P_g-(p_{air}-\rho_w gz)\right) \tag{13}$$

If the DA EOM is used for an incompressible fluid, it is reduced to the Lamb EOM.

3.5.2 Coupled GH-DA EOM

The coupled GH-DA EOM [8] is the GH-DA approach with migration motion coupled to the bubble radius EOM. The dilatation and migration EOM are shown in Eqs. (14) and (15) respectively.

$$R\ddot{R}+\frac{3}{2}\dot{R}^2-\frac{1}{4}\dot{z}^2=\rho_w^{-1}\left(\left(1+\frac{\dot{R}}{c}\frac{d}{dt}\right)P_g-(p_{air}-\rho_w gz)\right) \tag{14}$$

$$R\left[1+\frac{R}{c}\frac{d}{dt}\right]\ddot{z}+3\dot{R}\dot{z}-\frac{3}{4}C_D\dot{z}^2=2gR\left(1-\frac{\rho_c a_c^3}{\rho_w R^3}\right) \tag{15}$$

It was found that the inclusion of compressibility $\left(\frac{\dot{R}}{c}\frac{d}{dt}\right)$ in the migration EOM has a very small or negligible effect; therefore it was not included for this study.

3.5.3 GH-DAA EOM

The GH-DAA EOM [9], Eq. (16), is the only analytical expression that takes into account wave effects in both the external fluid and the gas bubble. This model does not account for migration of the gas bubble.

$$\begin{aligned} &R\ddot{R}\left(1+\zeta-\left(1-\frac{\rho_g}{\rho_l}\right)\frac{\dot{R}}{c}\right)+\frac{3}{2}\dot{R}^2\left(1+\frac{2}{3}\zeta-\frac{1}{3}\frac{\dot{R}}{c_l}+\frac{1}{3}\left(\frac{\rho_g}{\rho_l}\right)\left(1+\frac{\dot{R}}{c_l}+\frac{R}{c_l}\cdot\frac{\dot{\rho}_g}{\rho_g}\right)\right)+\left(\zeta c_l+\dot{\zeta}R\right)\dot{R} \\ &=\rho_w^{-1}\left(\left(p_{gas}-p_{air}+\rho_l gz\right)\left(1+\frac{\dot{R}}{c_l}\right)+\frac{R}{c_l}\dot{P}_g\right) \end{aligned} \tag{16}$$

Where $\zeta=\rho_g c_g/\rho_l c_l$ is the specific-acoustic-impedance ratio and subscripts *l* and *g* indicate the water and gas bubble respectively. The GH-DAA EOM reduces to that of Keller and Kolodner if the wave effects in the gas are not included. This is achieved by setting $\rho_g=\dot{\rho}_g=\zeta=\dot{\zeta}=0$ in Eq. (16). Including only the wave effects in the gas are achieved by setting $\zeta=0,\ c_l\to\infty$ and $\zeta c_l=\left(\rho_g/\rho_l\right)c_g$ in Eq. (16). This model cannot be implemented with incompressible fluids unless all wave effects are removed within the fluid and gas bubble, which was not considered in this study.

3.6 Modified Geers-Hunter (TNO) EOM

Based on the theory of the Geers-Hunter DA EOM, van Aanhold [2] developed analytical EOM for the dilatation and migration of the UNDEX gas bubble. These will be referred to as the TNO EOM within this report, and are shown in their general form in Eqs. (17) and (18) for the dilatation and migration motion respectively.

$$\left(\frac{3}{5}W+4\pi\rho_w R^3\right)\ddot{R}=-6\pi\rho_w R^2\dot{R}^2+K\pi\rho_w R^2\dot{z}^2+4\pi R^2\left(\left(1+\frac{\dot{R}}{c_l}\frac{d}{dt}\right)P_g-p_{air}+\rho_w gz\right) \tag{17}$$

$$\left(W+\frac{2}{3}\pi\rho_w R^3\right)\ddot{z}=\left(\frac{4}{3}\pi\rho_w R^3-W\right)g-2\pi\rho_w R^2\dot{R}\dot{z}+\frac{\pi}{2}\rho_w C_D R^2\dot{z}\left|\dot{z}\right| \tag{18}$$

Compared to the DA EOM, additions by van Aanhold include:

- A kinetic energy coupling switch, K. This couples the kinetic energy of the dilatation motion to the migration motion

- Gas inertia effect in the dilatation and migration motions, shown by inclusion of the charge weight, W, in the acceleration terms.

Similar to the other models that have been developed for compressible fluids, the TNO EOM can be used for an incompressible fluid by setting $c_l \to \infty$. The kinetic energy coupling between the dilatation and migration motions can be turned off by setting $K = 0$.

3.7 Equation of State

The equation of state is used to calculate the pressure within the gas bubble throughout the growth and collapse cycles. It is desirable to have an adiabatic equation of state (EOS) for the ease of calculations. Previous studies carried out by Jones and Miller (JM EOS) [11] and Lee, Horning, and Kury (JWL EOS) [12] who extended the work of Lee and Miller developed adiabatic EOS for dense gas. Both of these forms produced consistent models for the adiabatic expansion of the gas bubble for densities in the range of 1.0-1.63 g/cm^3 and at pressures below 100 MPa. For these conditions the EOS can be simplified to the ideal-gas form given by Eq. (19), which is implemented due to its simplicity compared to the more advanced JM and JWL EOS.

$$P_g = \lambda K \left(\frac{V_c}{V_g} \right)^{\gamma} = \lambda K \left(\frac{R_c}{R_g} \right)^{3\gamma} \tag{19}$$

where P is the pressure within the gas bubble, λ is the same energy loss function that is applied to the similitude plus energy loss models, K is the adiabatic charge constant, V is the bubble volume, R is the bubble radius, γ is the constant ratio of specific heats, subscript g denotes the gas bubble, and subscript c denotes the initial charge. For compressible fluid models the energy loss function is always equal to 1. For incompressible fluid models the energy loss function is the same as it is for the similitude models.

The adiabatic charge constant and ratio of constant specific heats for the incompressible fluid models can be determined from either the JM or JWL EOS. Due to the energy loss associated with the compressible fluid models, the charge constant for compressible fluid models must be significantly larger than that for incompressible fluids. Similar to van Aanhold [2], the charge constant for the compressible fluid models in this study were selected such that the first bubble radius and period agree reasonably well with the first cycle of the similitude equations. The ratio of constant specific heats is the same as that used for the incompressible fluid models.

4 Solution Methods

4.1 Similitude Equations

The similitude equations provide three approaches for calculating the radial and migration motion time histories with Eqs. (4) through (6). One uses these equations without energy losses; the second employs the energy loss function as described in Section 2.2.

The third approach uses the experimental results published by Swift and Decius [1] to directly calculate the radius and period of each bubble cycle, referred to as the "Exp. Fit" model. At the first gas bubble minimum the similitude constants are changed to the values for the second cycle. The same approach is used at the second gas bubble minimum. For the experimental cases which did not have best fits for the first three gas bubble cycles, the average values shown in Table 1 were used. This approach produces results that are very close to, and can be considered to be identical to, the experimental measurements.

4.2 Analytical Equations of Motion

The EOM for the analytical models in Eqs. (8) through (18) are nonlinear second-order differential equations that need to be solved by numerical integration. If the EOM can be expressed in the first order form $\dot{y} = f(y,t)$, the numerical solution is obtained using a fourth-order Runge-Kutta method [13], which has the basic form as shown in Eqs. (20) and (21).

$$y_{i+1} = y_i + \Delta t\left[\frac{1}{6}f(y_i,t_i) + \frac{1}{3}f\left(y^*_{i+1/2},t_{i+1/2}\right) + \frac{1}{3}f\left(y^{**}_{i+1/2},t_{i+1/2}\right) + \frac{1}{6}f\left(y^*_{i+1},t_{i+1}\right)\right] \tag{20}$$

where y_i is the variable at the start of the time step, Δt is the time step, and $f(y,t)$ is the first order differential variable evaluated at y and t.

$$\begin{aligned} y^*_{i+1/2} &= y_i + \frac{\Delta t}{2}f(y_i,t_i) \\ y^{**}_{i+1/2} &= y_i + \frac{\Delta t}{2}f\left(y^*_{i+1/2},t_{i+1/2}\right) \\ y^*_{i+1} &= y_i + \Delta t\, f\left(y^{**}_{i+1/2},t_{i+1/2}\right) \end{aligned} \tag{21}$$

A second order differential equation (DE) is reduced to a series of first order DEs by creating a dummy variable, in this example q, identical to the radial velocity of the gas bubble. The dummy variable is substituted into the original DE. Eq. (22) shows how this is done to produce two first order equations for the Lamb EOM.

$$f_1(q,t) = \dot{q} = \frac{1}{R}\left[\rho_w^{-1}\left(p_{gas} - p_{air} + \rho_w g z\right) - \frac{3}{2} q^2 \right]$$
$$f_2(q,t) = \dot{R} = q \tag{22}$$

The first order differential equations are solved with the initial conditions to determine $f(y_i, t_i)$. Initially the gas bubble is at rest with an initial radius equal to the initial charge radius, such that $R = R_c$, $\dot{R} = q = \dot{q} = 0$. $f(y_i, t_i)$ is then substituted into Eq. (21) to solve for $y^*_{i+1/2}$. This value is used to update all variables such as bubble pressure. Eq. (22) is used with the updated variables to determine $f\left(y^*_{i+1/2}, t_{i+1/2}\right)$. This process is repeated using Eqs. (21) and (22) to determine $y^{**}_{i+1/2}$ and $f\left(y^{**}_{i+1/2}, t_{i+1/2}\right)$. Eqs. (21) and (22) are used to determine y^*_{i+1} and $f\left(y^*_{i+1}, t_{i+1}\right)$. Eq. (20) was used to obtain y_{i+1} and the process is repeated for the next time step. The Runge-Kutta subroutine for the Lamb EOM is shown in Appendix B. It was found that a time step size of 5.0x10-7 seconds resulted in convergence, and this was therefore used for the numerical integration.

For the Lamb EOM the same energy loss function as that used for the similitude equations is applied during the calculations to reduce the adiabatic charge constant by the factors given by Eq. (7). Without the use of the energy loss function, there would be no reduction in the peak bubble radius throughout the time history. For the compressible fluid models the energy loss is inherent within the EOM, so there was no additional energy loss mechanism considered for this study.

4.3 Constants

The Swift and Decius [1] report gives no indication of the charge density or any other material properties other than the charge type. For this reason two sets of charge constants were used for comparison purposes. Cole [14] uses a gas exponent, $\gamma = 1.25$ for TNT, and therefore this was considered for one property set. The adiabatic charge constant, *K*, was selected to get reasonable agreement between the first bubble period and maximum radius for the compressible and incompressible (Lamb EOM) fluid cases. The second set of constants is those used by van Aanhold [2] in his study. The constants used for the analytical models are shown in Table 2.

Table 2: Constants used for solving the analytical models

Variables		Set 1	Set 2
Explosive Density, ρ_c (kg/m^3)		1500	1630
Gas exponent, γ		1.25	4/3
Adiabatic charge constant (MPa), K	Compressible	1350	2455
	Incompressible	740	1050
Drag Coefficient, C_d		2.25	2.25
Density of seawater (kg/m^3), ρ_w or ρ_l		1025	1025
Sound velocity in water (m/s), c		1500	1500
Acceleration of gravity (m/s^2), g		9.80665	9.80665
Air pressure (kPa), P_{air}		101.325	101.325

4.4 Code Development

The visualization software IDL was used to develop a code for calculating the gas bubble radius and migration, and the time histories for each of the analytical and similitude approaches. A different subroutine was developed for each of the similitude and analytical models. For the purpose of this study only the radial and migration displacements have been output from the subroutines, but could easily be changed to output all required variables.

5 Analytical and Similitude Results

This section compares the radial motion time history for the different similitude approaches as well as the various analytical models.

5.1 Similitude Energy Loss Model vs. Experimental Fit Model

Figure 2 shows a comparison of the experimental measurements and the energy loss function used in conjunction with the similitude equations.

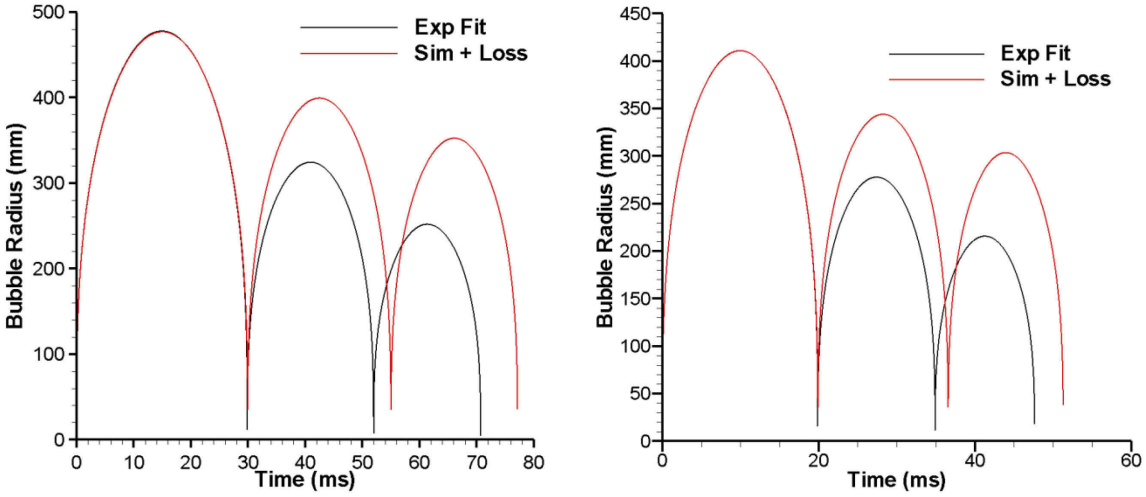

Figure 2: Comparison of experimental similitude response and similitude with energy loss function (a) Case G5F (b) Case G70F

From Figure 2 it can be seen that the energy loss function does not provide the required amount of reduction in the bubble period or radius. The energy loss function will result in a period and radius reduction of approximately 16 percent for the second bubble cycle and an additional 10 percent for the third bubble cycle. From the experimental fit it was found that on average the gas bubble period is reduced by approximately 25 percent and another 11 percent over the first and second bubble cycles respectively. The bubble radius over the first and second bubble cycles are reduced by 32 and 15 percent respectively.

5.2 Analytical Models

The following sections compare the bubble radius time history for the various analytical models, including the effect of fluid compressibility and the charge properties on the radius time history. Figure 3(a) shows a typical gas bubble migration time history. Due to the small bubble migration, less than 1 percent of the total depth, the coupling of

bubble depth and radius had a negligible effect on the gas bubble radius time histories, as shown by Figure 3(b).

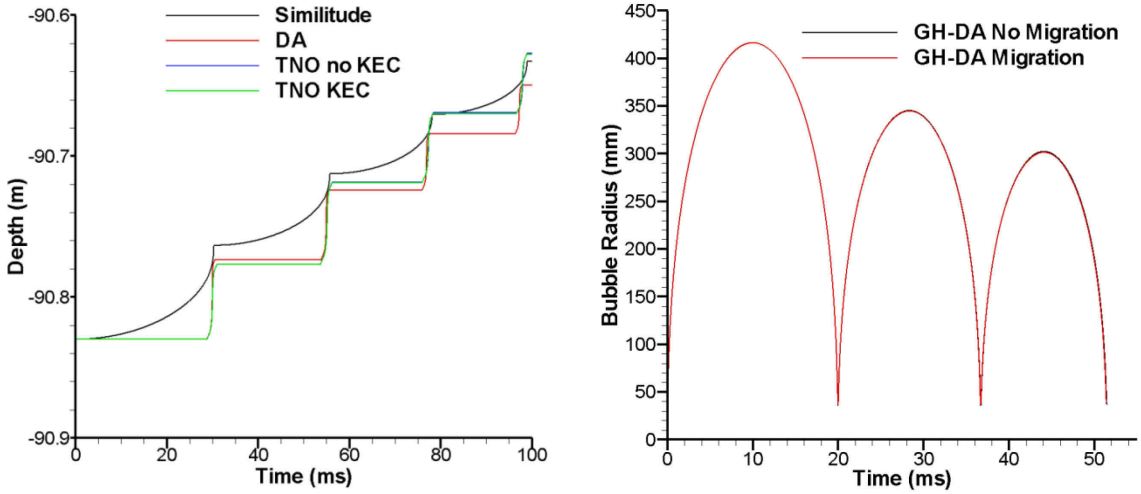

(a) (b)

Figure 3: Effect of including bubble migration in the analytical model (a) Typical gas bubble migration (b) Radius for a migration + dilatation model and dilatation only

5.3 Effect of Fluid Compressibility

Figure 4 shows the bubble radius time history of all analytical models for the depth and charge size for test case G5F. Figure 4(a) shows that all compressible gas models reduce to the Lamb EOM when the fluid becomes incompressible.

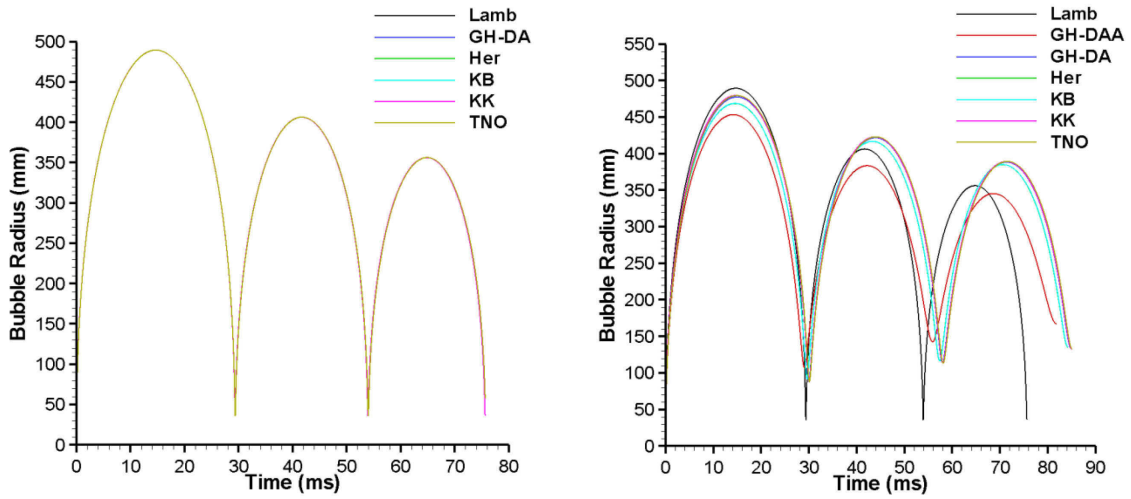

(a) (b)

Figure 4: Comparison of analytical bubble radius time history for a charge size and detonation depth equivalent to test G17F(a) Incompressible Fluid (b) Compressible Fluid

Figure 4(b) shows a comparison of all the analytical models with the water considered as a compressible fluid, with the exception of the Lamb EOM which does not have any compressible fluid modelling capability. These results are grouped according to compressibility. Considering just water compressibility the various models show little variation for a detonation depth of 93 m. The only models that show a significant difference are the Lamb EOM which does not consider water compressibility and the Geers-Hunter DAA (GH-DAA) model which includes compressibility in the water and the gas bubble. The additional energy loss factors considered in the GH-DAA formulation significantly reduces the maximum gas bubble radius and period when compared to the other analytical approaches.

5.4 Analytical Models vs. Experimental Fit Model

Figure 5 through Figure 8 compares analytical models with experimental fit results. GiF indicates the use of the similitude constants for the i^{th} test number from Swift and Decius [1]. Exp Fit indicates the experimental fit constants for all three bubble cycles are used. Sim + Loss indicates the first bubble cycle similitude constants are used along with the energy loss function. For the analytical models it is the name of the model followed by the property set from Table 2, where Prop1 indicates property set 1 and Prop2 is for property set 2.

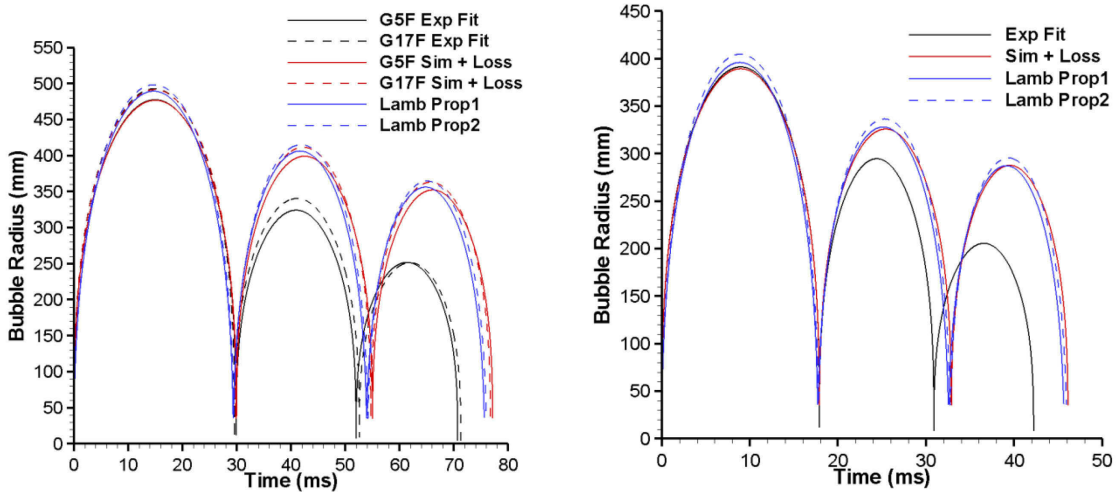

Figure 5: Comparison of experimental similitude response and the Lamb EOM with energy loss function (a) 93 m depth (b) 179 m depth

From Figure 5 it can be seen that the general behaviour of the Lamb EOM follows that of the similitude equation, with a slight improvement in the bubble period predictions for the Lamb EOM. The same energy loss function is applied to both of these models. The energy loss function does not provide the required energy reduction for the Lamb EOM as the peak radii and bubble periods of the experimental fits are significantly less.

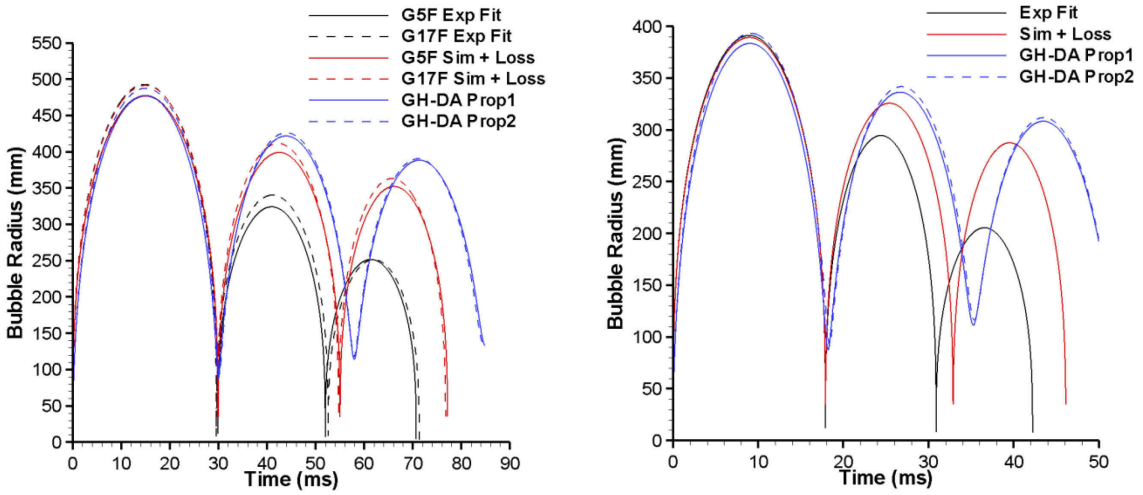

Figure 6: Comparison of experimental similitude response and the GH-DA EOM (a) 93 m depth (b) 179 m depth

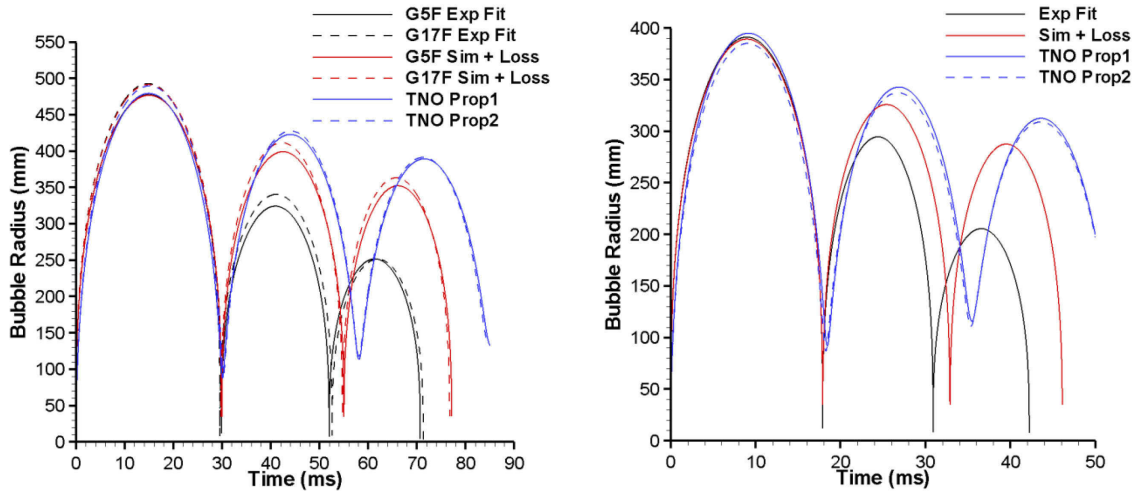

Figure 7: Comparison of experimental similitude response and the TNO EOM (a) 93 m depth (b) 179 m depth

Comparing Figure 6 and Figure 7 shows that including the gas inertia effects in the TNO EOM results in negligible differences in the gas bubble behaviour at the depths considered. These figures also show that the energy loss inherent within these models is not sufficient compared to the similitude plus energy loss or experimentally fit results. The compressible fluid models over predict the radii by 27 and 54 percent for the second and third gas bubble maximums and the periods by 11 and 19 percent compared to the experimental fit results.

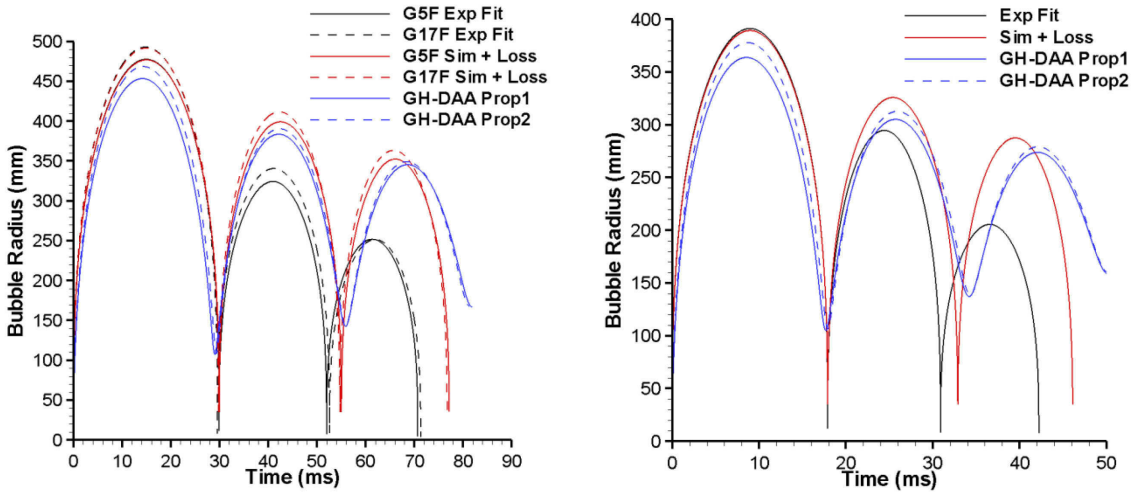

Figure 8: Comparison of experimental similitude response and the GH-DAA EOM (a) 93 m depth (b) 179 m depth

Figure 8 shows that the energy loss inherent within the DAA EOM formulation produces slightly better bubble radius results than that shown by the Lamb EOM and significantly better results than the other compressible fluid models. The bubble period predicted by the DAA EOM is not as large as that imposed by the energy loss function however it is larger than that produced by the other compressible fluid analytical models.

In general the two property sets have only a minor effect on the later bubble cycles, as shown by the convergence of the time histories during the third bubble cycle.

6 Conclusion

An extensive study on the analytical equations of motion available for predicting the gas bubble behaviour was conducted to determine which models and assumptions provide better predictions. Using the visualization software IDL the various analytical models and similitude equations, a code was developed. This code outputs the radial and migration time history for the various equations of motion and similitude approaches.

This study has shown that although the general gas bubble behaviour is captured by each of the analytical models there are still significant gaps in the predictions. It was found that the energy loss function proposed by van Aanhold [2] does not adequately predict the actual loss that occurs in the experiments when used in conjunction with the incompressible fluid models. It is also apparent that the energy loss inherent in the compressible fluid models does not fully predict the energy loss observed in experiments. The percent error in the gas bubble period and maximum bubble radii, compared to the experimental fits for a detonation depth of approximately 93 m and over 150 m, are shown in Table 3 and Table 4 respectively. The compressible EOM columns are the average of the various models that consider only compressibility in the surrounding fluid.

Table 3: Percent error in the gas bubble periods and maximum radii predicted by the analytical models compared to the experimental fits for a detonation depth of approximately 93 m

Cycle Number	Lamb EOM (%)		Compressible EOM (%)		GH-DAA EOM (%)	
	Period	Radius	Period	Radius	Period	Radius
1st	1.32	1.64	1.01	1.60	2.39	6.59
2nd	3.10	22.3	10.9	27.1	6.78	15.4
3rd	6.47	41.5	19.6	54.5	15.2	37.2

Table 4: Percent error in the gas bubble periods and maximum radii predicted by the analytical models compared to the experimental fits for a detonation depth of over 150 m

Cycle Number	Lamb EOM (%)		Compressible EOM (%)		GH-DAA EOM (%)	
	Period	Radius	Period	Radius	Period	Radius
1st	1.01	1.19	1.86	1.75	1.24	7.01
2nd	5.33	11.3	14.2	14.3	10.6	3.55
3rd	8.13	39.7	22.8	50.2	19.1	33.2

As these numbers show the Lamb EOM predicts the bubble period closer to the experimental fits than the other models. This shows that the energy loss function provides a larger loss than those inherent within the compressible fluid and GH-DAA EOM. As would be expected the GH-DAA model which accounts for fluid and gas bubble compressibility shows a significantly larger energy loss than the EOM considering compressibility in the fluid.

Table 3 and Table 4 show that there is a requirement to include an energy loss function in conjunction with the compressible fluid models. All models that include only the

compressibility in the fluid produce results very similar to one another; therefore a single energy loss function could be developed for all of these models. However, further studies would have to be conducted to determine if the energy loss is consistent for a range of detonation depths and charge types and sizes. The detonation depth is expected to be a significant factor for models that include coupling between radial motion and migration for shallow charges.

A concern of the approach used in this report is the method of determining the adiabatic charge constant for the compressible fluid models. The charge constant required for a compressible fluid is much larger than that used for incompressible models in order to get reasonable agreement for the first gas bubble period and maximum radius. This is due to the energy losses inherent in the compressible fluid models. The concern is that the gas constant is taken as a value that fits the first cycle of the gas bubble. A method that is proposed by Geers and Hunter [9] involves starting from a time shortly after detonation, and involves determining the bubble growth during the shock-wave phase. This approach allows for the use of the gas constant determined from the equations of state to be used for the compressible gas models. This approach will be introduced into the models in the future.

References

[1] Swift, E., and Decius, J.C. (1948), 'Measurements of bubble pulse phenomena III. Radius and period studies' in *Underwater Explosion Research* (Office of Naval Research, Washington, D.C., 1950), Vol. 2, 553-599.

[2] Van Aanhold, J.E. (2010), Simplified models for close-proximity UNDEX, TNO-034-DTM-2009-04888, TNO report, CONFIDENTIAL.

[3] Lamb, H. (1923), 'The early stages of a submarine explosion', Philos. Mag., 45 (Ser 6), 257-265.

[4] Herring, C. (1941), 'Theory of the pulsation of the gas bubble produced by an underwater explosion, in *Underwater Explosion Research* (Office of Naval Research, Washington, D.C., 1950), Vol. 2, 35-131.

[5] Kirkwood, J.G., and Bethe, H. (1942), 'The pressure wave produced by an underwater explosion I. (OSRD no. 588)' in *Shock and Detonation Waves*, edited by W.W. Wood (Gordon and Breach, New York, 1967), 1-34.

[6] Keller, J.B., and Kolodner, I.I. (1956), 'Damping of underwater explosion bubble oscillations', *J. Applied Phys.*, 27, 1152-1161.

[7] Geers, T.L., and Hunter, K.S. (1996), 'Dilatation dynamics of an underwater explosion bubble', *67th Shock and Vibration Symposium,* Monterey, CA, USA.

[8] Hunter, K.S., 1996, Underwater explosion bubble dynamics, M.Sc. Thesis, University of Colorado, Boulder, CO, USA.

[9] Geers, T.L., and Hunter, K.S. (2002), An integrated wave-effects model for an underwater explosion bubble, *J. Acoust. Soc. Am.*, 111 (4), 1584-1601.

[10] Prosperetti, A., and Lezzi, A. (1986), 'Bubble dynamics in a compressible liquid I. First-order Theory, *J. Fluid Mech.*, 168, 457-478.

[11] Jones, H., and Miller, A.R. (1948), 'The detonation of solid explosives', *Proc. R. Soc. London*, Ser. A 194A, 480-507.

[12] Lee, E.L., Hornig, H.C., and Kury, J.W. (1968), 'Adiabatic expansion of high explosive detonation products', Technical report UCRL-50422, Lawrence Livermore National Laboratory, Livermore, CA.

[13] Hornbeck, R.W. (1975), Numerical Methods, Englewood Cliffs, N.J.; Toronto, Ont.: Prentice-Hall, 310.

[14] Cole, R.H. (1948), Underwater Explosions, Princeton University Press, Princeton, 437.

This page intentionally left blank.

Annex A Swift and Decius Experimental Results

The following tables show the gas bubble periods and maximum gas bubble radius for the experiments conducted by Swift and Decius. Where the values in the shaded cells were calculated based on the average Ki_5 value, where i indicates the cycle number.

Table 5: Gas bubble period from experiments conducted by Swift and Decius [1].

Test Case	Charge Weight (lb)	Depth (ft)	First Period (msec)	$K1_5$	Second Period (msec)	$K2_5$	Third Period (msec)	$K3_5$
G1F	0.651	343	27.4	4.43	20.1	3.25	17.0	2.75
G2F	0.660	304	29.8	4.38	22.1	3.25	18.7	2.75
G4F	0.660	304	30.0	4.41	22.1	3.25	18.7	2.75
G5F	0.662	305	29.9	4.40	22.1	3.25	18.7	2.75
G6F	0.658	304	29.9	4.41	22.1	3.25	18.7	2.75
G7F	0.669	298	30.2	4.36	22.6	3.26	19.1	2.75
G8F	0.663	304	29.8	4.38	22.7	3.33	18.8	2.75
G9F	0.651	304	29.6	4.38	22.3	3.30	18.7	2.75
G17F	0.660	305	29.6	4.38	23.0	3.40	18.7	2.75
G18F	0.660	302	29.6	4.32	21.6	3.16	19	2.77
G20F	0.660	538	19.6	4.47	13.9	3.16	12.1	2.75
G21F	0.651	593	19.1	4.73	14.1	3.49	11.9	2.94
G23F	0.658	567	18.1	4.32	13.3	3.17	10.7	2.54
G70F	0.660	503	19.9	4.30	15.0	3.25	12.7	2.75
G71F	0.658	463	21.0	4.26	14.9	3.01	13.6	2.75
G72F	0.660	586	17.9	4.36	13.0	3.17	11.3	2.75
G73F	0.655	576	18.2	4.38	13.5	3.25	11.4	2.75
G74F	0.660	556	18.1	4.24	13.9	3.25	11.8	2.75
G76F	0.660	587	17.7	4.33	13.3	3.25	11.3	2.75
Average Values				4.36		3.25		2.75

Table 6: Maximum gas bubble radius from experiments conducted by Swift and Decius[1].

Test Case	Charge Weight (lb)	Depth (ft)	First R_{max} (in)	$K1_6$	Second R_{max} (in)	$K2_6$	Third R_{max} (in)	$K3_6$
G1F	0.651	343	18.1	12.6	12.2	8.50	9.50	6.60
G2F	0.660	304	18.8	12.5	12.8	8.50	9.90	6.60
G4F	0.660	304	18.8	12.5	12.8	8.50	9.90	6.60
G5F	0.662	305	18.8	12.5	12.8	8.50	9.90	6.60
G6F	0.658	304	18.8	12.5	13.2	8.80	9.90	6.60
G7F	0.669	298	18.9	12.4	12.7	8.40	10.0	6.60
G8F	0.663	304	18.9	12.5	12.8	8.50	9.90	6.60
G9F	0.651	304	18.7	12.5	11.4	7.60	10.0	6.70
G17F	0.660	305	19.4	12.9	13.4	8.90	9.90	6.60
G18F	0.660	302	19.4	12.8	12.1	8.00	10.6	7.00
G20F	0.660	538	15.9	12.6	10.6	8.40	8.20	6.50
G21F	0.651	593	15.7	12.9	9.90	8.10	7.90	6.50
G23F	0.658	567	15.6	12.6	9.90	8.00	7.80	6.30
G70F	0.660	503	16.2	12.6	10.9	8.50	8.50	6.60
G71F	0.658	463	16.6	12.6	11.0	8.30	8.70	6.60
G72F	0.660	586	15.4	12.5	11.6	9.50	8.10	6.60
G73F	0.655	576	15.6	12.7	10.5	8.50	8.10	6.60
G74F	0.660	556	15.7	12.6	10.6	8.50	8.20	6.60
G76F	0.660	587	15.1	12.3	11.6	9.50	8.10	6.60
Average Values				12.6		8.50		6.60

Annex B Runge-Kutta Code for the Lamb EOM

Step 1) Reduced differential equation to series of first order differential equations

$$LAMB\,EOM:\ R\ddot{R}+\frac{3}{2}\dot{R}^2=\rho_w^{-1}\left(p_{gas}-p_{air}+\rho_w gz\right)$$

reduces to:

$$f1=\dot{q}=\frac{1}{R}\left[\rho_w^{-1}\left(p_{gas}-p_{air}+\rho_w gz\right)-\frac{3}{2}q^2\right],\ f2=\dot{R}=q$$

Step 2) Calculate $f(y_i,t_i)$ using initial conditions $t = 0,\ \dot{q}=q=0$, $R=R_c$:

f11 = *calculate_f1_LAMB_EOM*(a, rho_w, P_g, gamma, R_c, P_amb, q, K, scale)
f21 = *calculate_f2_LAMB_EOM*(q)

where *f11* and *f21* are *f1* and *f2* at the initial conditions respectively. The *calculate_fi_LAMB_EOM*() is the call to the subroutines that calculate the functions *f1* and *f2*. The variables in the brackets are values passed into the subroutines.

Step 3) Calculate the $y^*_{i+1/2}$ values using $f(y_i,t_i)$:

q11 = *calculate_var*(q, dt/2.0, f11)
a11 = *calculate_var*(a, dt/2.0, f21)

where q11 and a11 are the $y^*_{i+1/2}$ for *f1* and *f2* respectively. *q11* and *a11* are the updated radial velocity and radius of the gas bubble respectively. *calculate_var()* is the subroutine developed to calculate the variables.

Step 4) Calculate $f\left(y^*_{i+1/2},t_{i+1/2}\right)$ using **Step 3** results

f12 = *calculate_f1_LAMB_EOM*(a11, rho_w, Pg, gamma, Ro, P_amb, q11, K, scale)
f22 = *calculate_f2_LAMB_EOM*(q11)

Step 5) Calculate the $y^{**}_{i+1/2}$ values using $f\left(y^*_{i+1/2},t_{i+1/2}\right)$:

q12 = *calculate_var*(q, dt/2.0, f12)
a12 = *calculate_var*(a, dt/2.0, f22)

Step 6) Calculate $f\left(y^{**}_{i+1/2},t_{i+1/2}\right)$ using **Step 5** values for *q* and *a*

f13 = *calculate_f1_LAMB_EOM*(a12, rho_w, Pg, gamma, Ro, P_amb, q12, K, scale)
f23 = *calculate_f2_LAMB_EOM*(q12)

Step 7) Calculate the y^*_{i+1} values using $f\left(y^{**}_{i+1/2},t_{i+1/2}\right)$:

q13 = *calculate_var*(q, dt, f13)
a13 = *calculate_var*(a, dt, f23)

Step 8) Calculate $f\left(y^{*}_{i+1}, t_{i+1}\right)$ using **Step 7** values for q and a:

f14 = *calculate_f1_LAMB_EOM*(a13, rho_w, Pg, gamma, Ro, P_amb, q13, K, scale)
f24 = *calculate_f2_LAMB_EOM*(q13)

Step 9) Calculate the variables at the end of the time step using Eq. as:

$$q_{i+1} = y_i + \Delta t\left[\frac{1}{6}f11 + \frac{1}{3}f12 + \frac{1}{3}f13 + \frac{1}{6}f14\right] = \dot{R}_{i+1}$$

$$a_{i+1} = y_i + \Delta t\left[\frac{1}{6}f21 + \frac{1}{3}f22 + \frac{1}{3}f23 + \frac{1}{6}f24\right] = R_{i+1}$$

Step 10) Repeat steps 2-9 for each time step.

List of symbols/abbreviations/acronyms/initialisms

a_c or R_c	Charge radius
c	Speed of sound in water
C_d	Drag coefficient
CFD	Computational fluid dynamics
D or d	Depth of charge detonation
DE	Differential equation
DND	Department of National Defence
DRDC	Defence Research & Development Canada
DRDKIM	Director Research and Development Knowledge and Information Management
EOM	Equation of motion
EOS	Equation of state
ft	Feet
g	Gravitational constant
JM	Jones miller equation of state
JWL	Jones-Wilkins-Lee equation of state
K	Adiabatic charge constant
K_5	Similitude constant for the first gas bubble period
K_6	Similitude constant for the maximum gas bubble radius
KB	Kirkwood and Bethe equation of motion
Kg	Kilograms
KK	Keller and Kolodner equation of motion
lb	Pounds
m	Cycle counter in energy loss function (m=0,1,2,3,...)
MFP	Maritime force protection
p_{air}	Atmospheric pressure at water surface
P_g	Internal gas bubble pressure
$\dot{P}_g$	Time rate of change of internal gas bubble pressure
R or R_g	Gas bubble radius

$\dot{R}$	Gas bubble radial velocity
$\ddot{R}$	Gas bubble radial acceleration
R&D	Research & Development
t	Time
T_b	Gas bubble period
TNO	The Netherlands Organisation for Applied Scientific Research (Nederlandse Organisatie voor Toegepast Natuurwetenschappelijk Onderzoek) Built Environment and Geosciences, Centre for Mechanical and Maritime Structures Organization
TNT	Trinitrotoluene
UNDEX	Underwater explosion
V	Gas bubble volume
V_c	Charge volume
V_g	Gas bubble volume
V_o	Initial gas bubble volume
V_{max}	Maximum first cycle gas bubble volume
W	Charge weight
z	Gas bubble depth
Δd	Explosive gas bubble vertical migration
ζ	Specific acoustic impedance ratio
γ	Gas exponent
λ	Energy loss function
π	Numerical value of pi
ρ_c	Charge density
ρ_g	Gas bubble density
ρ_l or ρ_w	Water density

Distribution list

Document No.: DRDC Atlantic TM 2010-237

LIST PART 1: Internal Distribution by Centre

4 Author (2 paper copies, 2 CD's)
1 PM/MFPTDP (1 CD)
3 Library (2 CDs, 1 paper copy)
1 H/TD
1 H/WP Scientific Authority
2 GL/ NPSS (1 CD, 1 paper copy)

12 TOTAL LIST PART 1

LIST PART 2: External Distribution within Canada by DRDKIM

1 Library and Archives Canada (Attn: Military Archivist, Government Records Branch)

1 NDHQ/DRDKIM

1 Laura Ozimek
Directorate Science & Technology Maritime
Defence Research & Development Canada
305 Rideau, St.
Ottawa, ON K1A 0K2

1 Cdr D. Sims
National Defence Headquarters
DGMEPM/DMSS 2
555 Blvd de la Carriere
Hull, PQ K1A 0K2

1 Dr. Julian Lee
DRDC Suffield
P. O. Box 4000 Stn Main
Medicine Hat, AB T1A 8K6

5 TOTAL LIST PART 2

List Part 3: External Distribution outside Canada by DRDKIM

1 Adrian van der Made
Head Vulnerability & Construction
Defence Material Organisation
Van der Burchlaan 31
PO Box 90822 MPC 58A
2509 LV The Hague, The Netherlands

1 J.E. van Aanhold
TNO Built Environment and Geosciences
Van Mourik Broekmanweg 6
2628 XE Delft The Netherlands

1 J. M. Luyten
TNO Defence, Security and Safety
Lange Kleiweg 137
2288 GJ Rijswijk
The Netherlands

1 Niklas Alin
FOI - Swedish Defence Research Agency
Grindsjon Research Centre
SE-147 25 Tumba, Sweden

4 TOTAL LIST PART 3

21 TOTAL COPIES REQUIRED

DOCUMENT CONTROL DATA

(Security classification of title, body of abstract and indexing annotation must be entered when the overall document is classified)

1. ORIGINATOR (The name and address of the organization preparing the document. Organizations for whom the document was prepared, e.g. Centre sponsoring a contractor's report, or tasking agency, are entered in section 8.)

Defence R&D Canada – Atlantic
9 Grove Street
P.O. Box 1012
Dartmouth, Nova Scotia B2Y 3Z7

2. SECURITY CLASSIFICATION (Overall security classification of the document including special warning terms if applicable.)

UNCLASSIFIED

3. TITLE (The complete document title as indicated on the title page. Its classification should be indicated by the appropriate abbreviation (S, C or U) in parentheses after the title.)

Analytical Solutions for Predicting Underwater Explosion Gas Bubble Behaviour

4. AUTHORS (last name, followed by initials – ranks, titles, etc. not to be used)

Riley, M.J.

5. DATE OF PUBLICATION (Month and year of publication of document.)	6a. NO. OF PAGES (Total containing information, including Annexes, Appendices, etc.)	6b. NO. OF REFS (Total cited in document.)
November 2010	42	14

7. DESCRIPTIVE NOTES (The category of the document, e.g. technical report, technical note or memorandum. If appropriate, enter the type of report, e.g. interim, progress, summary, annual or final. Give the inclusive dates when a specific reporting period is covered.)

Technical Memorandum

8. SPONSORING ACTIVITY (The name of the department project office or laboratory sponsoring the research and development – include address.)

Defence R&D Canada – Atlantic
9 Grove Street
P.O. Box 1012
Dartmouth, Nova Scotia B2Y 3Z7

9a. PROJECT OR GRANT NO. (If appropriate, the applicable research and development project or grant number under which the document was written. Please specify whether project or grant.)	9b. CONTRACT NO. (If appropriate, the applicable number under which the document was written.)

10a. ORIGINATOR'S DOCUMENT NUMBER (The official document number by which the document is identified by the originating activity. This number must be unique to this document.)	10b. OTHER DOCUMENT NO(s). (Any other numbers which may be assigned this document either by the originator or by the sponsor.)
DRDC Atlantic TM 2010-237	

11. DOCUMENT AVAILABILITY (Any limitations on further dissemination of the document, other than those imposed by security classification.)

Unlimited

12. DOCUMENT ANNOUNCEMENT (Any limitation to the bibliographic announcement of this document. This will normally correspond to the Document Availability (11). However, where further distribution (beyond the audience specified in (11) is possible, a wider announcement audience may be selected.))

13. ABSTRACT (A brief and factual summary of the document. It may also appear elsewhere in the body of the document itself. It is highly desirable that the abstract of classified documents be unclassified. Each paragraph of the abstract shall begin with an indication of the security classification of the information in the paragraph (unless the document itself is unclassified) represented as (S), (C), (R), or (U). It is not necessary to include here abstracts in both official languages unless the text is bilingual.)

This study describes different analytical models that have previously been developed for predicting the radial growth and collapse of underwater explosion (UNDEX) gas bubbles in a free-field environment. The report describes the implementation of nine analytical gas bubble models, in the form of nonlinear differential equations, and a fourth-order Runge-Kutta solution method. Gas bubble radius time histories calculated with these models are compared to empirical models derived from published experimental data. The analytical models allow for different assumptions such as fluid compressibility, bubble migration coupled to dilatation, and an empirical correction for energy loss. It was found that none of the analytical models fully account for the reduction in the gas bubble radius throughout the growth and collapse cycles. Including compressibility in the fluid and the gas bubble provides the best predictions when compared to experimental fits. The incompressible fluid model requires an empirical energy loss function, as there is no energy loss inherent within the model. Models considering just the compressibility of the surrounding fluid do not account for the full energy loss seen in the experimental fits, and produced similar results. Inclusion of migration effects had no influence on the bubble radius or period because of the large detonation depth.

La présente étude décrit différents modèles analytiques élaborés antérieurement pour prévoir la croissance et l'implosion radiales en champ libre des bulles gazeuses créées par une explosion sous-marine (UNDEX). Le rapport décrit la mise en œuvre de neuf modèles analytiques de bulles gazeuses utilisant des équations différentielles non linéaires et une méthode de solution de Runge-Kutta du quatrième ordre. On compare l'évolution temporelle du rayon des bulles gazeuses calculée avec ces divers modèles avec celle obtenue avec des modèles empiriques dérivés de données expérimentales publiées. Les modèles analytiques permettent différentes hypothèses concernant, entre autres, la compressibilité du fluide, la migration des bulles reliée à la dilatation, et la correction empirique de la perte d'énergie. On constate qu'aucun des modèles analytiques ne peut expliquer complètement la réduction du rayon des bulles gazeuses sur toute l'étendue des cycles de croissance et d'implosion. L'inclusion des compressibilités du fluide et des bulles gazeuses donne les meilleures prévisions comparativement aux ajustements avec les données expérimentales. Le modèle à fluide incompressible exige d'utiliser une fonction empirique de perte d'énergie étant donné qu'il ne tient pas compte lui-même de la perte d'énergie. Les modèles qui ne tiennent compte que de la compressibilité du fluide environnant ne peuvent expliquer complètement la perte d'énergie observée dans les ajustements aux données expérimentales et donnent des résultats similaires. L'inclusion des effets dus à la migration n'a aucun effet sur le rayon ou la durée des bulles à cause de la grande profondeur à laquelle les explosions ont lieu.

14. KEYWORDS, DESCRIPTORS or IDENTIFIERS (Technically meaningful terms or short phrases that characterize a document and could be helpful in cataloguing the document. They should be selected so that no security classification is required. Identifiers, such as equipment model designation, trade name, military project code name, geographic location may also be included. If possible keywords should be selected from a published thesaurus, e.g. Thesaurus of Engineering and Scientific Terms (TEST) and that thesaurus identified. If it is not possible to select indexing terms which are Unclassified, the classification of each should be indicated as with the title.)

Underwater Explosion, gas bubble, migration, analytical models, similitude

This page intentionally left blank.

Defence R&D Canada

Canada's leader in defence
and National Security
Science and Technology

R & D pour la défense Canada

Chef de file au Canada en matière
de science et de technologie pour
la défense et la sécurité nationale

www.drdc-rddc.gc.ca